

# Solar neutrinos: Near-far asymmetry and just-so oscillations

B. Faïd<sup>c</sup>, G. L. Fogli<sup>b</sup>, E. Lisi<sup>a,b</sup>, and D. Montanino<sup>b</sup>

<sup>a</sup>*Institute for Advanced Study, Princeton, New Jersey 08540*

<sup>b</sup>*Dipartimento di Fisica dell'Università and Sezione INFN, I-70126 Bari, Italy*

<sup>c</sup>*Institut de Physique, Université des Sciences et de la Technologie, DZ-16111 Algiers, Algeria*

## Abstract

We propose to study possible signals of just-so oscillations in new-generation solar neutrino experiments by separating the events detected when the earth is nearest to the sun (perihelion  $\pm 3$  months) from those detected when the earth is farthest from the sun (aphelion  $\pm 3$  months). We introduce a solar model independent near-far asymmetry, which is non-zero if just-so oscillations occur. We apply our calculations to the kinetic energy spectra of electrons induced by  $^8\text{B}$  solar neutrino interactions in the SuperKamiokande and Sudbury Neutrino Observatory experiments. We show that the sensitivity to the neutrino oscillation parameters can be increased by probing the near-far asymmetry in selected parts of the electron energy spectra.

PACS number(s): 26.65.+t, 14.60.Pq, 13.15.+g.

## I. INTRODUCTION

Neutrino flavor oscillations in vacuum [1–3] represent a viable solution [4–9] to the observed deficit of the solar neutrino flux [10–13] as compared to the predictions of the standard solar model [14,15].

If the oscillations have a wavelength comparable to the earth orbit radius (just-so oscillations [4]), then significant distortions could arise both in the neutrino energy spectrum [16–18] (as a result of the energy-dependence of the oscillation probability) and in the time structure of the signal [19,18,7] (as a result of the earth’s orbit eccentricity [20]). The combination of these two effects, namely time-dependent spectral distortions, could also be observable [4,18].

The four pioneering solar neutrino experiments have not observed such effects. The three radiochemical experiments [10–12] cannot observe *a priori* spectral distortions since they detect only energy-integrated signals [16], and do not show evidence for periodic variations of the detected rates associable to just-so oscillations (see, e.g., [5,7]). The neutrino-electron scattering experiment Kamiokande [13] shows no evidence for distortions in the spectrum of the scattered electrons [21] either. However, these are low-statistics experiments, and possible vacuum oscillation effects could be hidden by the relatively large uncertainties.

Much higher statistics (thousands of events per year) will be collected with the second-generation experiments SuperKamiokande [22,23] and Sudbury Neutrino Observatory (SNO) [24,25]. These real-time experiments can test variations in the time structure of the signal, as well as deviations of the solar neutrino energy spectrum from its standard shape. In particular, information about the  $^8\text{B}$  solar neutrino spectrum  $\lambda(E)$  [26] can be gained through the observation of the electron spectrum [14] from the reactions

$$\nu + e^- \rightarrow \nu' + e^- \text{ (SuperKamiokande)}, \quad (1)$$

$$\nu_e + d \rightarrow p + p + e^- \text{ (SNO)} . \quad (2)$$

In this work we study a specific signal of just-so oscillations which involves both time variations and shape distortions of the electron kinetic energy spectrum expected at SuperKamiokande and SNO. We propose to separate the events detected when the earth is nearest to the sun (perihelion  $\pm 3$  months) from those detected when the earth is farthest from the sun (aphelion  $\pm 3$  months). In Sec. II we introduce a near-far asymmetry  $A_{NF}$ , which is non-zero if just-so oscillations occur. In Sec. III and IV we apply our calculations of  $A_{NF}$  to the kinetic energy spectra of electrons in the SuperKamiokande and SNO experiments respectively. We show how the sensitivity to the neutrino oscillation parameters can be increased by probing the near-far asymmetry in selected parts of the electron energy spectra. In Sec. V we summarize our work and draw our conclusions. Some technical aspects of our calculations are discussed in the Appendices A and B.

## II. NEAR-FAR ASYMMETRY $A_{NF}$ : GENERAL

In this section we define the near-far asymmetry  $A_{NF}$ , introduce briefly the notation for two-family and three-family neutrino oscillations, and express  $A_{NF}$  as a function of the neutrino mass-mixing parameters. Details of the calculation are reported in Appendix A.

### A. Definition of $A_{NF}$

The earth orbit radius,  $\ell$ , varies periodically around its average value,  $L = 1.496 \times 10^8$  km, according to

$$\ell = L(1 - \varepsilon \cos \vartheta) + \mathcal{O}(\varepsilon^2) , \quad (3)$$

where  $\varepsilon = 0.0167$  is the orbit eccentricity, and

$$\vartheta \equiv \frac{2\pi t}{T} \quad (4)$$

is the orbital phase ( $T = 1$  yr,  $t = 0$  at the perihelion). Variations of  $\ell$  with the neutrino production point in the sun are negligible for our purposes (see Appendix B).

Along the earth's orbit, the intercepted neutrino flux  $\Phi$  varies as:

$$\Phi \propto \frac{L^2}{\ell^2} = 1 + 2\varepsilon \cos \vartheta + \mathcal{O}(\varepsilon^2) . \quad (5)$$

Let us divide the orbit in two parts, a “near” half (centered at the perihelion, january 4th) and a “far” half (centered at the aphelion, july 4th):

$$\begin{aligned} \text{“near” semi-orbit} &= \text{perihelion} \pm 3 \text{ months} \\ &\Rightarrow \vartheta \in [-\pi/2, \pi/2] , \end{aligned} \quad (6a)$$

$$\begin{aligned} \text{“far” semi-orbit} &= \text{aphelion} \pm 3 \text{ months} \\ &\Rightarrow \vartheta \in [\pi/2, 3\pi/2] . \end{aligned} \quad (6b)$$

If no oscillations occur, the flux of solar  $\nu_e$  is subject only to a geometrical variation [Eq. (5)]. In this case, the integrated neutrino rate in the near semi-orbit is enhanced by a geometric factor  $1 + 4\varepsilon/\pi$ :

$$\frac{1}{\pi} \int_{-\pi/2}^{\pi/2} d\vartheta \frac{L^2}{\ell^2} = 1 + \frac{4\varepsilon}{\pi} + \mathcal{O}(\varepsilon^2) . \quad (7)$$

Analogously, the integrated neutrino rate in the far semi-orbit is suppressed by a geometric factor  $1 - 4\varepsilon/\pi$ .

It is useful to factorize out this overall geometric correction from the observations and define<sup>1</sup>

---

<sup>1</sup> In principle, a real-time signal could be instantaneously corrected for the geometric factor  $L^2/\ell^2$ , if also the background were known in real time and subtracted. However, background subtraction is better defined for time-integrated signals. Therefore, we prefer to factorize the half-year averaged geometric correction  $1 \pm 4\varepsilon/\pi$  from the integrated rate, instead of factorizing the instantaneous correction  $L^2/\ell^2$  from the real-time rate.

$$N = \frac{\text{No. of events in the near semi-orbit}}{1 + 4\varepsilon/\pi} , \quad (8a)$$

$$F = \frac{\text{No. of events in the far semi-orbit}}{1 - 4\varepsilon/\pi} . \quad (8b)$$

“Event” is referred here to as the observation of a solar neutrino induced electron. The relevant reactions are Eq. (1) for SuperKamiokande (neutrino scattering) and Eq. (2) for SNO (neutrino absorption). Both experiments can measure the kinetic energy,  $T$ , of the scattered or recoil electrons through the Cherenkov light. The “No. of events” in Eq. (8) may refer either to the whole electron energy spectrum,  $s(T)$ , or to a selected part of it. The first option has the advantage of higher statistics; the second is useful to study possible time-dependent spectral distortions. The formalism that will be used in Sections II B and II C is the same in both cases. Further specifications about the electron energy spectrum will be made in Sections III and IV.

We define a near-far asymmetry as

$$A_{NF} = \frac{N - F}{N + F} . \quad (9)$$

The statistical error of  $A_{NF}$ , as derived by applying the binomial statistics to the “near” and “far” classes of events, is  $1/\sqrt{N_{\text{tot}}}$ , where  $N_{\text{tot}} = N + F$ . Systematic errors can be expected to cancel to a large fraction in a ratio of rates such as  $(N - F)/(N + F)$ .

The asymmetry  $A_{NF}$  is zero if no neutrino oscillations occur, or if oscillations independent of  $\ell$  take place. Therefore, a non-zero value of  $A_{NF}$  would be a signature of just-so oscillations. Notice that  $A_{NF}$  is independent of the solar model and, in particular, of the absolute  $^8\text{B}$  neutrino flux.

## B. Vacuum oscillations: Notation

In the presence of just-so oscillations, the asymmetry  $A_{NF}$  is a function of the neutrino mass-mixing parameters. We consider two cases: two-family ( $2\nu$ ) oscillations, and three-family ( $3\nu$ ) oscillations with only one relevant mass scale.

In the two-family case, the electron neutrino  $\nu_e$  is a mixture of two mass eigenstates  $\nu_1$  and  $\nu_2$ , with masses  $m_1$  and  $m_2$  respectively:

$$\nu_e = c_\omega \nu_1 + s_\omega \nu_2 , \quad (10)$$

$$\delta m^2 = |m_2^2 - m_1^2| , \quad (11)$$

where  $\omega$  is the  $\theta_{12}$  mixing angle,  $s_\omega = \sin \omega$ , and  $c_\omega = \cos \omega$ .

The  $\nu_e$  survival probability,  $P^{2\nu} = P^{2\nu}(\nu_e \rightarrow \nu_e)$ , is then given by

$$P^{2\nu} = 1 - 2s_\omega^2 c_\omega^2 + 2s_\omega^2 c_\omega^2 \cos k\ell , \quad (12)$$

where

$$k = \frac{2\pi}{\lambda_\nu} = \text{wave number} , \quad (13)$$

$$\lambda_\nu = \frac{4\pi E}{\delta m^2} = \text{oscillation length} , \quad (14)$$

and  $E$  is the neutrino energy.

In the case of three-family neutrino oscillations, the state  $\nu_e$  is a mixture of  $\nu_1$ ,  $\nu_2$ , and  $\nu_3$ :

$$\nu_e = c_\phi c_\omega \nu_1 + c_\phi s_\omega \nu_2 + s_\phi \nu_3 , \quad (15)$$

where  $\omega = \theta_{12}$  and  $\phi = \theta_{13}$  in the standard parametrization of the mixing matrix [27,28].

We make the simplificative hypothesis that the mass gap between  $\nu_3$  and the doublet ( $\nu_1, \nu_2$ ) is very large:  $m^2 \equiv |m_3^2 - m_1^2| \gg |m_2^2 - m_1^2| \equiv \delta m^2$ . This hypothesis holds, for instance, if one assumes that  $m^2$  is in the range ( $\gtrsim 10^{-3} \text{ eV}^2$ ) probed by accelerator, reactor, and atmospheric neutrino experiments [29]. With this assumption the  $m^2$ -driven fast oscillations are averaged away, and the  $3\nu$  survival probability is given by (see, e.g., [29])

$$P^{3\nu} = c_\phi^4 P^{2\nu} + s_\phi^4 , \quad (16)$$

with  $P^{2\nu}$  as in Eq. (12).

A useful representation of the  $3\nu$  parameter space ( $\delta m^2, \omega, \phi$ ) has been given in [30] in terms of a “unitarity triangle.” We refer the reader to [30] for a description of this representation, which will be used to display some of the results in Sections III and IV.

In summary:

$$\text{no oscillations} \Rightarrow A_{NF} = 0 , \quad (17a)$$

$$2\nu \text{ oscillations} \Rightarrow A_{NF}^{2\nu} = A_{NF}^{2\nu}(\delta m^2, \omega) , \quad (17b)$$

$$3\nu \text{ oscillations} \Rightarrow A_{NF}^{3\nu} = A_{NF}^{3\nu}(\delta m^2, \omega, \phi) . \quad (17c)$$

In the next Section we give explicit formulas for Eqs. (17b) and (17c).

### C. Calculation of $A_{NF}$

The rates  $N$  and  $F$  in Eq. (8) are integrated over a half-year and over all, or part, of the electron energy spectrum. It follows that the calculation of  $A_{NF}$  involves a time integration over the near and far semiorbits, as well as an energy integration weighted by the  $^8\text{B}$  neutrino spectrum,  $\lambda(E)$ , and by the  $\nu_e$  and  $\nu_x$  ( $x \neq e$ ) cross sections,  $\sigma_e(E)$  and  $\sigma_x(E)$  respectively.

In the calculation, we discard terms of  $\mathcal{O}(\varepsilon^2)$ , but we keep all powers in  $\varepsilon kL$  since  $kL$  may be large. We also neglect the very small smearing effect over the neutrino production region (see Appendix B).

It turns out that the time integration in the two semiorbits can be done analytically, leaving only a numerical integration over  $E$  to be performed. We refer the reader to Appendix A for the derivation of the final results, that can be expressed in compact form as

$$A_{NF}^{2\nu} = \frac{2s_\omega^2 c_\omega^2 G(\delta m^2)}{1 - 2s_\omega^2 c_\omega^2 F(\delta m^2)} , \quad (18)$$

for  $2\nu$  oscillations, and as

$$A_{NF}^{3\nu} = \frac{2c_\phi^4 s_\omega^2 c_\omega^2 G(\delta m^2)}{1 - 2s_\phi^2 c_\phi^2 R - 2c_\phi^4 s_\omega^2 c_\omega^2 F(\delta m^2)} . \quad (19)$$

for  $3\nu$  oscillations.

The functions  $F(\delta m^2)$  and  $G(\delta m^2)$  and the factor  $R$  in Eqs. (18) and (19) are defined as

$$F(\delta m^2) = \frac{\int dE \lambda(E) [\sigma_e(E) - \sigma_x(E)] f(\delta m^2/E)}{\int dE \lambda(E) \sigma_e(E)} , \quad (20)$$

$$G(\delta m^2) = \frac{\int dE \lambda(E) [\sigma_e(E) - \sigma_x(E)] g(\delta m^2/E)}{\int dE \lambda(E) \sigma_e(E)} , \quad (21)$$

$$R = \frac{\int dE \lambda(E) [\sigma_e(E) - \sigma_x(E)]}{\int dE \lambda(E) \sigma_e(E)} , \quad (22)$$

where  $f$  and  $g$  are non-dimensional functions of  $\delta m^2/E$  ( $= 2k$ ):

$$f = 1 - cJ_0(\varepsilon kL) - 2\varepsilon sJ_1(\varepsilon kL) + \frac{4\varepsilon}{\pi} s\mathbf{H}_0(\varepsilon kL) , \quad (23)$$

$$g = \frac{4\varepsilon}{\pi} c + s\mathbf{H}_0(\varepsilon kL) - 2\varepsilon c\mathbf{H}_1(\varepsilon kL) - \frac{4\varepsilon}{\pi} cJ_0(\varepsilon kL) , \quad (24)$$

with  $s = \sin kL$ ,  $c = \cos kL$ . In Eqs. (23) and (24),  $J_{0,1}$  and  $\mathbf{H}_{0,1}$  are the Bessel and Struve functions [31,32] of order 0 and 1, respectively. Computer routines for the numerical calculation of these special functions can be found in [33].

Figure 1 shows the functions  $f$  and  $g$  in the relevant range  $\delta m^2/E \in [10^{-12}, 10^{-8}]$  eV<sup>2</sup>/MeV. These functions are detector-independent. The calculation of  $F$  and  $G$  from Eqs. (20) and (21) requires instead detector-dependent ingredients such as the interaction cross-sections. These ingredients are discussed in Sec. III and IV for SuperKamiokande and SNO, respectively.

### III. $A_{NF}$ IN SUPERKAMIOKANDE

In this section we calculate the expected values of  $A_{NF}$  for SuperKamiokande in the presence of  $2\nu$  and  $3\nu$  oscillations.

#### A. Detector parameters

The SuperKamiokande experiment [22] makes use of a 22 kton (fiducial volume) water-Cherenkov detector to observe the electrons scattered by solar neutrinos through reaction (1).

The *measured* kinetic energy of the electron,  $T$ , is expected to be distributed around the *true* electron energy,  $T'$ , according to the following energy resolution function [14]:

$$R(T, T') = \frac{1}{\Delta_{T'}\sqrt{2\pi}} \exp \left[ -\frac{(T - T')^2}{2\Delta_{T'}^2} \right], \quad (25)$$

where the energy-dependent one-sigma width  $\Delta_{T'}$  scales as  $\sqrt{T'}$  due to the photon statistics,

$$\Delta_{T'} = \Delta_{10} \sqrt{\frac{T'}{10 \text{ MeV}}}, \quad (26)$$

and the nominal width at 10 MeV is  $\Delta_{10} = 1.6 \text{ MeV}$  [22].

If the experiment works as expected, a high signal-to-noise ratio will be achieved for  $T \gtrsim 5 \text{ MeV}$  [34]. We adopt  $T_{\min} = 5 \text{ MeV}$  as a nominal threshold in our analysis.

## B. Neutrino cross-section and electron spectrum

The neutrino cross section for the reaction (1) is known to the first order in the radiative corrections [35], both for  $\nu = \nu_e$  and for  $\nu = \nu_x$  ( $x \neq e$ ).

The standard electron spectrum  $s(T)$  expected in SuperKamiokande in the absence of oscillations is given by

$$s(T) = \int dE \lambda(E) \int_0^{T'_{\max}} dT' R(T, T') \frac{d\sigma_e(E, T')}{dT'}, \quad (27)$$

where  $\lambda(E)$  is the neutrino spectrum,  $T'_{\max}$  is the maximum *true* kinetic energy allowed by kinematics [14],  $R(T, T')$  is given in Eq. (25), and  $d\sigma_e/dT'$  is the  $\nu_e$  differential cross section [14,35].

Figure 2 shows the standard spectrum  $s(T)$  for SuperKamiokande. As we will see in Sec. III C, it is also useful to consider selected parts of the electron energy spectrum (bins). An illustrative choice of bins is shown in Fig. 2. The first five bins have a width of 1 MeV. The sixth bin collects all events with  $T \geq 10 \text{ MeV}$ . In the presence of oscillations, we will calculate the asymmetry  $A_{NF}$  using both the total number of events in the spectrum, and the number of events collected in each of the six bins shown in Fig. 2. The loss of statistics is then traded for an increased sensitivity to the neutrino mass-mixing parameters (see Sec. III C).

It is useful to introduce a “reduced”  $\nu_e$  cross-section for the  $i$ -th bin,  $\sigma_{e,i}(E)$ , defined as the cross section for a  $\nu_e$  of energy  $E$  to produce an electron with a *measured* energy falling in the  $i$ -th bin range  $[T_{i,\min}, T_{i,\max}]$ :

$$\sigma_{e,i}(E) = \int_{T_{i,\min}}^{T_{i,\max}} dT \int_0^{T'_{\max}} dT' R(T, T') \frac{d\sigma(E, T')}{dT'} \quad (28)$$

An analogous definition can be given for the  $\nu_x$  reduced cross-sections,  $\sigma_{x,i}(E)$ .

The total cross section  $\sigma_e$  for producing an electron with measured energy above the nominal threshold ( $T_{\min} = 5 \text{ MeV}$ ) and including the finite energy resolution is:

$$\sigma_e(E) = \sum_{i=1}^6 \sigma_{e,i}(E) . \quad (29)$$

The total cross sections  $\sigma_e(E)$  and  $\sigma_x(E)$ , or the binned cross sections  $\sigma_{e,i}(E)$  and  $\sigma_{x,i}(E)$ , enter the calculation of  $A_{NF}$  through the integrals in Eqs.(20)–(22), where they are always weighted by the  $^8\text{B}$  neutrino spectrum  $\lambda(E)$ .

In Fig. 3 we show the products  $\lambda(E)\sigma_e(E)$  (upper panel) and  $\lambda(E)\sigma_{e,i}(E)$  (lower panel) as a function of  $E$ . The curve in the upper panel thus represents the  $\nu_e$  spectrum contribution to the whole electron spectrum in SuperKamiokande. Analogously, the curves in the lower panel represent the  $\nu_e$  spectrum contribution to each of the six bins shown in Fig. 2.<sup>2</sup> Notice that, although the width of the first five electron energy bins is 1 MeV, the corresponding width of the  $\lambda(E)\sigma_{e,i}(E)$  curves is much larger, indicating that there is no tight relation between the measured electron energy  $T$  and the energy  $E$  of the parent neutrino. This is due both to the smearing effect of the energy resolution function [Eq. (25)] and to the fact that the differential cross section  $d\sigma/dT$  for  $\nu$ - $e$  scattering is rather flat in  $T$  [14]. The finite energy resolution also allows non-zero values of  $\lambda(E)\sigma_{e,i}(E)$  for  $E < T_{i,\text{min}}$ . Nevertheless, from Fig. 3 we learn that it is possible to “tune,” to some extent, the typical neutrino energy relevant to  $A_{NF}$  by choosing the appropriate bin in the electron energy spectrum.

### C. $A_{NF}$ with $2\nu$ oscillations

Figure 4 shows curves of iso- $A_{NF}$  ( $\times 100$ ) for the unbinned (whole spectrum) case, in the presence of  $2\nu$  oscillations. The curves are displayed in the usual  $(\sin^2 2\omega, \delta m^2)$  plane, and are separated by steps of 0.5% in  $A_{NF}$ .

The maximum absolute value of  $A_{NF}$  ( $\sim 2.5\%$ ) is reached for  $\sin^2 2\omega \simeq 1$  and  $\delta m^2 \simeq 10^{-10} \text{ eV}^2$ . If the statistical errors dominate, a near-far effect of 2% could be detected at SuperKamiokande after the first year of operation.

The near-far asymmetry can be either positive or negative (solid and dotted curves, respectively). The positive (negative) values of  $A_{NF}$  correspond to an energy-averaged  $\nu_e$  survival probability  $\langle P \rangle$  decreasing (increasing) with the sun-earth distance.  $A_{NF}$  is  $\sim 0$  at the stationary points of  $\langle P \rangle$ , corresponding approximately to

$$L \simeq n \frac{\langle \lambda_\nu \rangle}{2} , \quad (30)$$

where  $\langle \lambda_\nu \rangle = 4\pi \langle E \rangle / \delta m^2$  is the oscillation length in terms of the typical neutrino energy  $\langle E \rangle$  ( $\sim 10 \text{ MeV}$  for Fig. 4) and  $n$  is an integer. The near-far asymmetry tends to zero also for large  $\delta m^2$  (fast oscillations), for very small  $\delta m^2$  (oscillation lengths much longer than  $L$ ), and for small  $\sin^2 2\omega$  (small neutrino mixing).

If Eq. (30) is fulfilled for a certain value of  $\delta m^2$ , no near-far asymmetry can be observed, independently of the value of  $\sin^2 2\omega$ . However, as noticed in the previous section, one can

---

<sup>2</sup> Curves of  $\lambda\sigma_x$  (not shown in Fig. 3) would be similar to the  $\lambda\sigma_e$  curves, but scaled by a factor  $\sim 1/6$  in height.



change the value of  $\langle E \rangle$  (and thus the position of the zeros of  $A_{NF}$ ) by selecting the events in a specific bin of the electron energy spectrum.

In Fig. 5 we show curves of iso- $A_{NF}$  calculated for the six bins indicated in Fig. 2. The typical neutrino energy increases from bin 1 to bin 6 (see Fig. 3) and correspondingly the sensitivity to higher  $\delta m^2$  increases. The positions of the zeros of  $A_{NF}$  are also shifted from bin to bin, so that by using two or more bins no “holes” in the  $\delta m^2$ -sensitivity are left. Notice that the near-far asymmetry can reach values as high as 3.5% in favorable cases of large mixing, and that the sensitivity to small mixing is increased in some bins.

The comparison of Figs. 4 and 5 shows that selecting some intervals (bins) of the electron energy spectrum helps to reach higher sensitivities to the neutrino oscillation parameters. Of course, the statistical (and possibly the systematic) uncertainties also increase when a subset of the total event sample is used. An optimal sensitivity-to-uncertainty ratio can be assessed only after the detector performances and the results of the SuperKamiokande experiment are known in detail.

#### D. $A_{NF}$ with $3\nu$ oscillations

As discussed in Sec. II B, we study  $3\nu$  oscillations in the simple case of one relevant mass scale. The corresponding parameter space  $(\delta m^2, \omega, \phi)$  can be represented, for any fixed value of  $\delta m^2$ , through the “triangular” representation introduced in [30].

Figure 6 shows curves of iso- $A_{NF}$  ( $\times 100$ ) in the triangular representation for  $\delta m^2 = 10^{-10}$  eV<sup>2</sup> and  $\delta m^2 = 5.5 \times 10^{-11}$ . The calculations refer to the unbinned case (whole spectrum). We recall [30] that a generic point in the triangle represents the electron-neutrino state  $\nu_e$ , while the upper, lower right, and lower left corners represent the mass eigenstates  $\nu_3$ ,  $\nu_2$ , and  $\nu_1$  respectively. The triangle is mapped by the (non-orthogonal) coordinates  $\sin^2 \omega$  and  $\sin^2 \phi$ . The asymmetry  $A_{NF}$  is maximal (in absolute value) on the lower side of the triangle, corresponding to pure  $2\nu$  oscillations between  $\nu_1$  and  $\nu_2$ . For  $\phi > 0$ , the  $\nu_e$ - $\nu_3$  mixing tends to suppress the near-far effect, since by hypothesis the oscillations driven by massive state  $\nu_3$  are so fast to be averaged out, giving a time-independent contribution. In short, in order to have a large near-far asymmetry for  $3\nu$  oscillations, the  $\omega$ -mixing must be maximal and the  $\phi$ -mixing must be relatively small.

In Fig. 6 we have shown only two representative values of  $\delta m^2$ . The range of  $\delta m^2$  to which  $A_{NF}$  is sensitive for  $3\nu$  oscillations would be practically the same as for  $2\nu$  oscillations. The zeros of  $A_{NF}^{3\nu}$  and  $A_{NF}^{2\nu}$  are also reached at the same values of  $\delta m^2$  [compare Eqs. (18) and (19)]. These “holes” in the  $\delta m^2$ -sensitivity can be “closed,” as in the  $2\nu$  case, by repeating the asymmetry measurement in selected bins of the electron energy spectrum.

### IV. $A_{NF}$ IN SNO

In this section we calculate the expected values of  $A_{NF}$  at SNO in the presence of  $2\nu$  and  $3\nu$  oscillations.

### A. Detector parameters

The SNO experiment [24] makes use of a 1 kton heavy-water Cherenkov detector to observe the recoil electrons from neutrino absorption in deuterium [Eq. (2)].

The discussion of the detector parameters would be very similar to SuperKamiokande (Sec. III A) and is not repeated here. We only report the adopted (expected) values for the resolution width at 10 MeV,  $\Delta_{10} = 1.1$  MeV, and for the energy threshold,  $T_{\min} = 5$  MeV [36].

### B. Neutrino cross section and electron spectrum

The cross section for neutrino absorption in deuterium has been studied in detail in several papers (see [37] and references therein). No relevant uncertainties are recognized at solar neutrino energies [37,36], apart from a  $\sim \pm 5\%$  error in the overall normalization that is irrelevant in a ratio of rates like  $A_{NF}$ . A computer code for the calculation of the  $\nu$ - $d$  differential cross section is available in [38].

The differential cross section  $d\sigma_e/dT$  for reaction (2) is sharply peaked in the electron energy (see, e.g., [36]). This feature represents a considerable advantage with respect to  $\nu$ - $e$  scattering in SuperKamiokande [reaction (1)], since it results in a tighter correlation between the electron energy  $T$  and the parent neutrino energy  $E$ .

Figure 7 shows the standard (i.e., no oscillation) electron spectrum for SNO. In Fig. 7 we also show, as in Fig. 3, the energy bins chosen to illustrate to near-far asymmetry effect in selected parts of the spectrum.

Figure 8 illustrates the  $T$ - $E$  correlation in SNO. This figure is analogous to Fig. 4, but with the appropriate SNO neutrino cross-sections (defined in analogy to Eq. (28)). By changing the electron energy bin, the spectrum  $\lambda(E)\sigma_e(E)$  of parents neutrinos contributing to that bin changes considerably. The corresponding variations in SuperKamiokande (Fig. 4) are less pronounced. Therefore we expect a greater sensitivity to near-far effects in SNO.

Another advantage of SNO is that the reaction (2) can be initiated only by electron neutrinos:  $\sigma_x = 0$  ( $x \neq e$ ). It follows that the factor  $R$  defined in Eq. (22) is equal to 1.

### C. $A_{NF}$ with $2\nu$ oscillations

Figure 9 shows curves of iso- $A_{NF}$  for SNO (unbinned case), in the  $2\nu$  oscillation plane ( $\sin^2 2\omega$ ,  $\delta m^2$ ). The contours are separated by steps of 1% in  $A_{NF}$ .

The shape of the curves in Fig. 9 is similar to Fig. 4, since the typical neutrino energy is  $\langle E \rangle \sim 10$  MeV as in SuperKamiokande. However, the absolute value of the asymmetry in SNO is about twice as large as in SuperKamiokande, because of the tighter correlation between the observed electron spectrum and the parent neutrino spectrum, as discussed in Sec. IV B. The maximum absolute value of  $A_{NF}$  is  $\sim 6.3\%$ .

Figure 10 shows curves of iso- $A_{NF}$  calculated for the six representative bins shown in Fig. 7. As for SuperKamiokande, we note that by changing bin the  $\delta m^2$ -position of the  $A_{NF}$  zeros changes, and higher sensitivities to low mixing angles can also be achieved.

A comparison of Figs. 4, 5, 9, and 10, shows that the SuperKamiokande and the SNO experiment can probe, through measurements of the near-far asymmetry, the range  $2.5 \times 10^{-11} \lesssim \delta m^2 \lesssim 9 \times 10^{-10} \text{ eV}^2$  for sufficiently large mixing.

#### D. $A_{NF}$ with $3\nu$ oscillations

Figure 11 shows curves of iso- $A_{NF}$  for SNO, in the presence of  $3\nu$  oscillations, for two representative values of  $\delta m^2$ .

In Fig. 11 the same triangular representation of Fig. 6 is used. The shape of the contours in Fig. 11 (SNO) and Fig. 6 (SuperKamiokande) are similar, but the near-far asymmetry is larger in the SNO experiment, for the same reason as in the  $2\nu$  case (see Sec. IV C).

### V. SUMMARY AND CONCLUSIONS

We have studied the signals of just-so oscillations that can be observed in the SuperKamiokande and SNO solar neutrino experiments by separating the events detected when the earth is nearest to the sun (perihelion  $\pm 3$  months) from those detected when the earth is farthest from the sun (aphelion  $\pm 3$  months).

We have calculated the asymmetry  $A_{NF}$  between the near and far signals by factorizing out the trivial geometrical variation of the signal, and using the entire electron energy spectrum as well as representative spectrum bins. The calculations involve the integration of the  $\nu_e$  survival probability over time and energy. The time integration over half-year can be performed analytically. Compact expressions for the near-far asymmetry have been given for  $2\nu$  and  $3\nu$  oscillations. The value of  $A_{NF}$  is solar model independent, and is different from zero if just-so oscillations occur.

In the case of  $2\nu$  oscillations, it has been shown that measurements of the near-far asymmetry at SNO and SuperKamiokande can probe the range  $2.5 \times 10^{-11} \lesssim \delta m^2 \lesssim 9 \times 10^{-10} \text{ eV}^2$  for sufficiently large values of the mixing angle  $\omega = \theta_{12}$ . A similar range of  $\delta m^2$  and  $\omega$  can be probed in the presence of  $3\nu$  oscillations with one relevant mass scale, provided that the second mixing angle  $\phi = \theta_{13}$  is not large.

The SNO experiment appears to be about twice as sensitive as SuperKamiokande to the near-far asymmetry, due to the different energetics of the  $\nu$ - $d$  absorption and  $\nu$ - $e$  scattering reactions.

In both experiments, measurements of  $A_{NF}$  in selected bins of the electron energy spectrum may increase the sensitivity to the neutrino oscillation parameters. Since the selection of a bin implies a loss of statistics, the net gain of binning the spectrum in measurements of  $A_{NF}$  can be assessed only after the experiments have run for some time and the data and their uncertainties are well understood.

### ACKNOWLEDGMENTS

We thank P. I. Krastev for useful discussions. One of us (B.F.) thanks the Dipartimento di Fisica and Sezione INFN di Bari for kind hospitality. The work of E.L. was supported

in part by INFN and in part by the Institute for Advanced Study through a Hansmann membership. This work has been performed under the auspices of the European Theoretical Astroparticle Network (TAN).

## APPENDIX A: TIME AND ENERGY INTEGRATION IN $A_{NF}$

In this Appendix we prove the basic Eqs. (18) and (19) for the near-far asymmetry.

In the presence of oscillations, the expected value of the quantity  $N$  in Eq. (8a) is given by the sum of the  $\nu_e$  and  $\nu_x$  contributions

$$N = \int dE \lambda(E) \sigma_e(E) \overline{P}_N(E) + \int dE \lambda(E) \sigma_x(E) (1 - \overline{P}_N(E)), \quad (\text{A1})$$

where  $E$  is the neutrino energy,  $\lambda(E)$  is the  $^8\text{B}$  neutrino spectrum,  $\sigma_e$  and  $\sigma_x$  are the  $\nu_e$  and  $\nu_x$  ( $x \neq e$ ) interaction cross-sections,<sup>3</sup> and  $\overline{P}_N$  is the  $\nu_e$  survival probability  $P(E, \vartheta)$  averaged over the near semiorbit:

$$\overline{P}_N(E) = \frac{\frac{1}{\pi} \int_{-\pi/2}^{\pi/2} d\vartheta \frac{L^2}{\ell^2} P(E, \vartheta)}{\frac{1}{\pi} \int_{-\pi/2}^{\pi/2} d\vartheta \frac{L^2}{\ell^2}}. \quad (\text{A2})$$

In the above equation,  $L^2/\ell^2$  is given by Eq. (5), and the denominator on the right hand side is equal to  $1 + 4\epsilon/\pi$  [Eq. (7)]. For  $P = P^{2\nu}$  or  $P = P^{3\nu}$  [Eqs. (12) and (15)] the numerator can be calculated analitically with the help of the following integrals [31,32]:

$$\frac{2}{\pi} \int_0^{\pi/2} d\vartheta \cos(x \cos \vartheta) = J_0(x), \quad (\text{A3})$$

$$\frac{2}{\pi} \int_0^{\pi/2} d\vartheta \sin(x \cos \vartheta) = \mathbf{H}_0(x), \quad (\text{A4})$$

$$\frac{2}{\pi} \int_0^{\pi/2} d\vartheta \cos \vartheta \sin(x \cos \vartheta) = J_1(x), \quad (\text{A5})$$

$$\frac{2}{\pi} \int_0^{\pi/2} d\vartheta \cos \vartheta \cos(x \cos \vartheta) = \frac{2}{\pi} - \mathbf{H}_1(x), \quad (\text{A6})$$

where  $J_n$  and  $\mathbf{H}_n$  are the Bessel and Struve functions [31,32] of order  $n$ :

---

<sup>3</sup> It is understood that the cross sections are already corrected for threshold and resolution effects in the electron spectrum. The cross sections may refer either to the entire electron spectrum (above threshold) or to a specific bin. See Secs. III B and IV B for details.

$$J_n(x) = \left(\frac{1}{2}x\right)^n \sum_{m=0}^{\infty} \frac{(-1)^m \left(\frac{1}{2}x\right)^{2m}}{\Gamma(m+1)\Gamma(n+m+1)} , \quad (\text{A7})$$

$$\mathbf{H}_n(x) = \left(\frac{1}{2}x\right)^{n+1} \sum_{m=0}^{\infty} \frac{(-1)^m \left(\frac{1}{2}x\right)^{2m}}{\Gamma(m+\frac{3}{2})\Gamma(n+m+\frac{3}{2})} . \quad (\text{A8})$$

In particular, in the  $2\nu$  oscillation case the result of the integration is:<sup>4</sup>

$$\begin{aligned} \frac{1}{\pi} \int_{-\pi/2}^{\pi/2} d\vartheta \frac{L^2}{\ell^2} P^{2\nu}(E, \vartheta) = \\ 1 + \frac{4\varepsilon}{\pi} - 2s_\omega^2 c_\omega^2 (1 - cJ_0 - 2\varepsilon sJ_1) \\ + 2s_\omega^2 c_\omega^2 \left[ s\mathbf{H}_0 - 2\varepsilon c\mathbf{H}_1 + \frac{4\varepsilon}{\pi}(c-1) \right] , \end{aligned} \quad (\text{A9})$$

where  $s = \sin kL$ ,  $c = \cos kL$ , and the argument of the functions  $J_n$  and  $\mathbf{H}_n$  is  $\varepsilon kL$ .

From Eqs. (A2), (A9), and (7), it follows that

$$\overline{P}_N^{2\nu} = 1 - 2s_\omega^2 c_\omega^2 (f - g) + \mathcal{O}(\varepsilon^2) , \quad (\text{A10})$$

where  $f$  and  $g$  are defined as in Eqs. (23) and (24). The function  $f$  ( $g$ ) is even (odd) in  $\varepsilon$ .

The analogous result for the far semiorbit can be simply obtained with the replacement  $\varepsilon \rightarrow -\varepsilon$ :

$$\overline{P}_F^{2\nu} = 1 - 2s_\omega^2 c_\omega^2 (f + g) + \mathcal{O}(\varepsilon^2) . \quad (\text{A11})$$

The derivation for the  $3\nu$  oscillation case is very similar to the  $2\nu$  case and gives:

$$\overline{P}_N^{3\nu} = c_\phi^4 + s_\phi^4 - 2c_\phi^4 s_\omega^2 c_\omega^2 (f - g) , \quad (\text{A12})$$

$$\overline{P}_N^{3\nu} = c_\phi^4 + s_\phi^4 - 2c_\phi^4 s_\omega^2 c_\omega^2 (f + g) . \quad (\text{A13})$$

Finally, we group the cross-sections and the probabilities in the expression of near-far asymmetry [see Eqs. (9) and (A1)]:

$$A_{NF} = \frac{\int dE \lambda(\sigma_e - \sigma_x)(\overline{P}_N - \overline{P}_F)}{2 \int dE \lambda \sigma_e + \int dE \lambda(\sigma_e - \sigma_x)(\overline{P}_N + \overline{P}_F - 2)} , \quad (\text{A14})$$

and divide the numerator and the denominator of the above fraction by  $\int dE \sigma_e$ . Then, using Eqs. (A10)–(A13) and the definitions in Eqs. (20)–(22) one easily obtains Eqs. (18) and (19).

---

<sup>4</sup> Terms of  $\mathcal{O}(\varepsilon^2)$  or higher are neglected. However, all powers of  $\varepsilon k\ell$  are kept, since  $\varepsilon k\ell$  can be of  $\mathcal{O}(1)$ .

## APPENDIX B: INTEGRATION OVER THE NEUTRINO PRODUCTION REGION

In the calculation of  $A_{NF}$  we have neglected the effect of smearing the  $\nu_e$  survival probability  $P$  over  $^8\text{B}$  neutrino production region in the sun [15]. Already in [1] it was recognized that this effect is negligible for just-so oscillations, since the typical oscillation length is much larger than the production region (see also [39]). Here we rederive and discuss this result in more detail.

Let us chart the neutrino production region with polar coordinates  $(r, \alpha)$ , where the angle  $\alpha$  is zero along the line joining the center of the sun ( $r \equiv 0$ ) to the detector. (The second polar angle is integrated out for the cylindrical symmetry of the problem.) The distance  $\ell'$  between the generic neutrino production point and the detector is then given by

$$\ell' = \ell - r \cos \alpha . \quad (\text{B1})$$

We find that the  $^8\text{B}$  neutrino source density in the standard solar model [15] is approximated very well by the following Gaussian distribution:

$$\rho(r) = \frac{1}{(2\pi\sigma^2)^{3/2}} \exp\left(-\frac{1}{2}\frac{r^2}{\sigma^2}\right) , \quad (\text{B2})$$

where  $\sigma = 0.0313 R_\odot$  ( $R_\odot = 6.96 \times 10^5 \text{ km}$ ). Since  $\sigma \ll R_\odot$ , one can effectively take  $r = \infty$  as upper limit in the radial integration, instead of  $r = R_\odot$ .

The normalization of  $\rho(r)$  is fixed by:

$$2\pi \int_{-1}^{+1} d\cos\alpha \int_0^\infty dr r^2 \rho(r) = 1 \quad (\text{B3})$$

Given Eq. (B1) and the functional form (B2) for  $\rho$ , the smearing of the neutrino oscillation factor  $\cos k\ell$  [Eq. (12)] over the production region can be performed analytically:

$$\begin{aligned} \langle \cos k\ell \rangle &\equiv 2\pi \int_{-1}^{+1} d\cos\alpha \int_0^\infty dr r^2 \rho(r) \cos k\ell' \\ &= e^{-\frac{1}{2}k^2\sigma^2} \cos k\ell \end{aligned} \quad (\text{B4})$$

Therefore, the damping effect of the spatial smearing on the oscillating term can be absorbed in the exponential suppression factor of Eq. (B4). For  $E = 5 \text{ MeV}$  and  $\delta m^2$  as high as  $10^{-9} \text{ eV}^2$ , this suppression factor differs from 1 by only  $6 \times 10^{-5}$ . Such a small difference is negligible for our purposes. The smearing correction is even smaller than the corrections of the order  $\varepsilon^2 = 2.8 \times 10^{-4}$ , which can also be neglected in the calculation of the near-far asymmetry.

## REFERENCES

- [1] B. Pontecorvo, Zh. Eksp. Teor. Fiz. **53**, 1717 (1967) [Sov. Phys. JETP **26**, 984 (1968); V. Gribov and B. Pontecorvo, Phys. Lett. B **28**, 493 (1969).
- [2] The idea of  $\nu_e$ - $\nu_\mu$  mixing [1] was independently introduced also by Y. Katayama, K. Matumoto, S. Tanaka, and E. Yamada, Prog. Theor. Phys. **28**, 675 (1962); Z. Maki, M. Nakagawa, and S. Sakata, *ibid.* **28**, 870 (1962).
- [3] S. Bilenky and B. Pontecorvo, Phys. Rep. **41**, 225 (1978).
- [4] S. L. Glashow and L. M. Krauss, Phys. Lett. B **190**, 199 (1987).
- [5] P. I Krastev and S. T. Petcov, Phys. Lett. B **285**, 85 (1992); *ibidem* **299**, 99 (1993); Phys. Rev. D **53**, 1665 (1996).
- [6] A. Acker, S. Pakvasa, and J. Pantaleone, Phys. Rev. D **43**, 1754 (1991); A. Acker, A. B. Balantekin, and F. Loreti, Phys. Rev. D **49**, 328 (1994).
- [7] E. Calabresu, N. Ferrari, G. Fiorentini, and M. Lissia, Astropart. Phys. **4**, 159 (1995).
- [8] Z. G. Berezhiani and A. Rossi, Phys. Lett. B **367**, 219 (1996).
- [9] J. N. Bahcall and P. I. Krastev, Phys. Rev. D **53**, 4211 (1996).
- [10] R. Davis, Prog. Part. Nucl. Phys. **32**, 13 (1994); B. T. Cleveland *et al.*, in *Neutrino '94*, Proceedings of the 16th International Conference on Neutrino Physics and Astrophysics, Eilat, Israel, edited by A. Dar, G. Eilam, and M. Gronau [Nucl. Phys. B (Proc. Suppl.) **31**, 47 (1995)].
- [11] GALLEX Collaboration, P. Anselmann *et al.*, Phys. Lett. B **357**, 237 (1995).
- [12] SAGE Collaboration, J. S. Nico *et al.*, in *ICHEP '94*, Proceedings of the 27th International Conference on High Energy Physics, Glasgow, Scotland, edited by P. J. Bussey and I. Knowles (Institute of Physics Publishing, Bristol, 1995) vol. II, p. 965; J. N. Abdurashitov *et al.*, Phys. Lett. B **328**, 234 (1994).
- [13] Kamiokande Collaboration, Y. Suzuki *et al.*, in *Neutrino '94* [10], p. 54; K. S. Hirata *et al.*, Phys. Rev. D **44**, 2241 (1991); **45**, 2170(E) (1992).
- [14] J. N. Bahcall, *Neutrino Astrophysics* (Cambridge University Press, Cambridge, 1989).
- [15] J. N. Bahcall and M. H. Pinsonneault, Rev. Mod. Phys. **67**, 781 (1995).
- [16] J. N. Bahcall and S. C. Frautschi, Phys. Lett. B **29**, 623 (1969).
- [17] V. Barger, K. Whisnant, and R. J. N. Phillips, Phys. Rev. D **24**, 538 (1981); *ibid.* **43**, 1110 (1991).
- [18] P. I. Krastev and S. T. Petcov, Nucl. Phys. B **449**, 605 (1995).
- [19] R. Ehrlich, Phys. Rev. D **18**, 2323 (1978).
- [20] I. Pomeranchuk, as cited in the second of Refs. [1].
- [21] Kamiokande Collaboration, K. S. Hirata *et al.*, Phys. Rev. Lett. **65**, 1301 (1990).
- [22] Y. Totsuka, in *TAUP '95*, Proceedings of the 4th International Workshop on Theoretical and phenomenological Aspects of Underground Physics, Toledo, Spain, edited by A. Morales, J. Morales, and J. A. Villar [Nucl. Phys. B (Proc. Suppl.) **48**, 547 (1996)]; A. Suzuki, in *Physics and Astrophysics of Neutrinos*, edited by M. Fukugita and A. Suzuki (Springer-Verlag, Tokyo, 1994), p. 414.
- [23] Current information on the status of the SuperKamiokande experiment can be retrieved from the following URL's: <http://www-sk.icrr.u-tokyo.ac.jp/> and <http://www.ps.uci.edu/~superk/>.
- [24] SNO Collaboration, G. T. Ewan *et al.*, "Sudbury Neutrino Observatory Proposal,"

- Report No. SNO-87-12, 1987 (unpublished); “Scientific and Technical Description of the Mark II SNO Detector,” edited by E. W. Beier and D. Sinclair, Queen’s University Report No. SNO-89-15, 1989 (unpublished); A. B. McDonald, Proceedings of the 9th Lake Louise Winter Institute, edited by A. Astbury *et al.* (World Scientific, Singapore, 1994), p. 1.
- [25] Current information on the status of the SNO experiment can be retrieved from the following URL: <http://snodaq.phy.queensu.ca/SNO/sno.html>.
  - [26] J. N. Bahcall, E. Lisi, D. E. Albarger, L. De Braekeleer, S. J. Freedman, and J. Napolitano, Phys. Rev. C **54**, 411 (1996).
  - [27] T. K. Kuo and J. Pantaleone, Phys. Lett. B **198**, 406 (1987).
  - [28] Particle Data Group, R. M. Barnett *et al.*, Phys. Rev. D **54**, 1 (1996).
  - [29] G. L. Fogli, E. Lisi, and D. Montanino, Phys. Rev. D **49**, 3626 (1994); Astropart. Phys. **4**, 177 (1995); G. L. Fogli, E. Lisi, and G. Scioscia, Phys. Rev. D **52**, 5334 (1995).
  - [30] G. L. Fogli, E. Lisi, and D. Montanino, Institute for Advanced Study Report No. IASSNS-AST 96/21, hep-ph/9605273, to be published in Phys. Rev. D.
  - [31] I. S. Gradshteyn and I. M. Ryzhik, *Tables of Integrals, Series, and Products* (Academic Press, San Diego CA, 1994).
  - [32] M. Abramowitz and I. A. Stegun, *Handbook of Mathematical Functions with Formulas, Graphs, and Mathematical Tables* (John Wiley & Sons, New York, 1972).
  - [33] CERN Program Library CERNLIB, routines C312 (Bessel functions) and C342 (Struve functions). A printable description of these routines can be found at the URL: <http://wwwcn.cern.ch/asdoc/cernlib.html>.
  - [34] Y. Totsuka and Y. Suzuki, private communication.
  - [35] J. N. Bahcall, M. Kamionkowski, and A. Sirlin, Phys. Rev. D **51**, 6146 (1995).
  - [36] J. N. Bahcall and E. Lisi, Institute for Advanced Study Report No. IASSNS-AST-96-33, hep-ph/9607433, to appear in Phys. Rev. D.
  - [37] K. Kubodera and S. Nozawa, Int. J. Mod. Phys. E **3**, 101 (1994).
  - [38] Computer program DIFFCROSS.FOR, available at the URL <http://www.sns.ias.edu/~jnb> (see Neutrino Export Software and Data).
  - [39] P. I. Krastev, Institute for Advanced Study Report No. IASSNS-AST 96/34.



## FIGURES

FIG. 1. The detector-independent functions  $f$  and  $g$  defined in the text.

FIG. 2. SuperKamiokande: Standard electron spectrum  $s(T)$  as a function of the measured electron kinetic energy  $T$ . The area under  $s(T)$  is normalized to 1. Also shown are the (numbered) energy bins used in the analysis of  $A_{NF}$ .

FIG. 3. SuperKamiokande: Spectra of  $\nu_e$  contributing to the entire standard electron spectrum of Fig. 2 or to selected bins. The neutrino spectra are weighted by the interaction cross sections, taking into account the detector threshold and the energy resolution function.

FIG. 4. SuperKamiokande: Curves of iso- $A_{NF}$  for  $2\nu$  oscillations (all bins).

FIG. 5. SuperKamiokande: Curves of iso- $A_{NF}$  for  $2\nu$  oscillations (separated bins).

FIG. 6. SuperKamiokande: Curves of iso- $A_{NF}$  for  $3\nu$  oscillations (all bins), for two representative values of  $\delta m^2$ . The triangular representation is discussed in the text.

FIG. 7. SNO: Standard electron spectrum  $s(T)$  as a function of the measured electron kinetic energy  $T$ . The area under  $s(T)$  is normalized to 1. Also shown are the (numbered) energy bins used in the analysis of  $A_{NF}$ .

FIG. 8. SNO: Spectra of  $\nu_e$  contributing to the entire standard electron spectrum of Fig. 7 or to selected bins. The neutrino spectra are weighted by the interaction cross sections, taking into account the detector threshold and the energy resolution function.

FIG. 9. SNO: Curves of iso- $A_{NF}$  for  $2\nu$  oscillations (all bins).

FIG. 10. SNO: Curves of iso- $A_{NF}$  for  $2\nu$  oscillations (separated bins).

FIG. 11. SNO: Curves of iso- $A_{NF}$  for  $3\nu$  oscillations (all bins), for two representative values of  $\delta m^2$ . The triangular representation is discussed in the text.

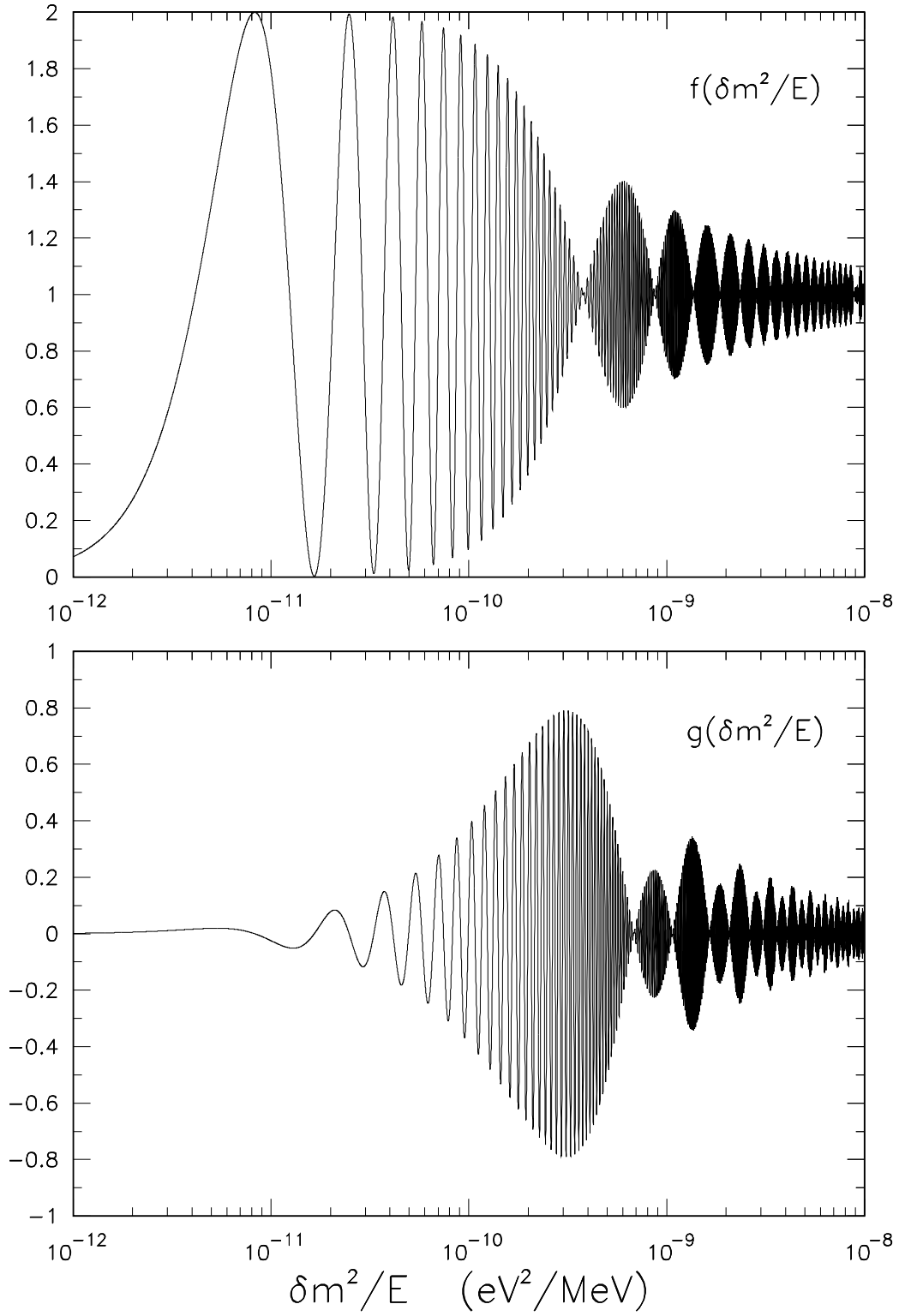


FIG. 1. The detector-independent functions  $f$  and  $g$  defined in the text.

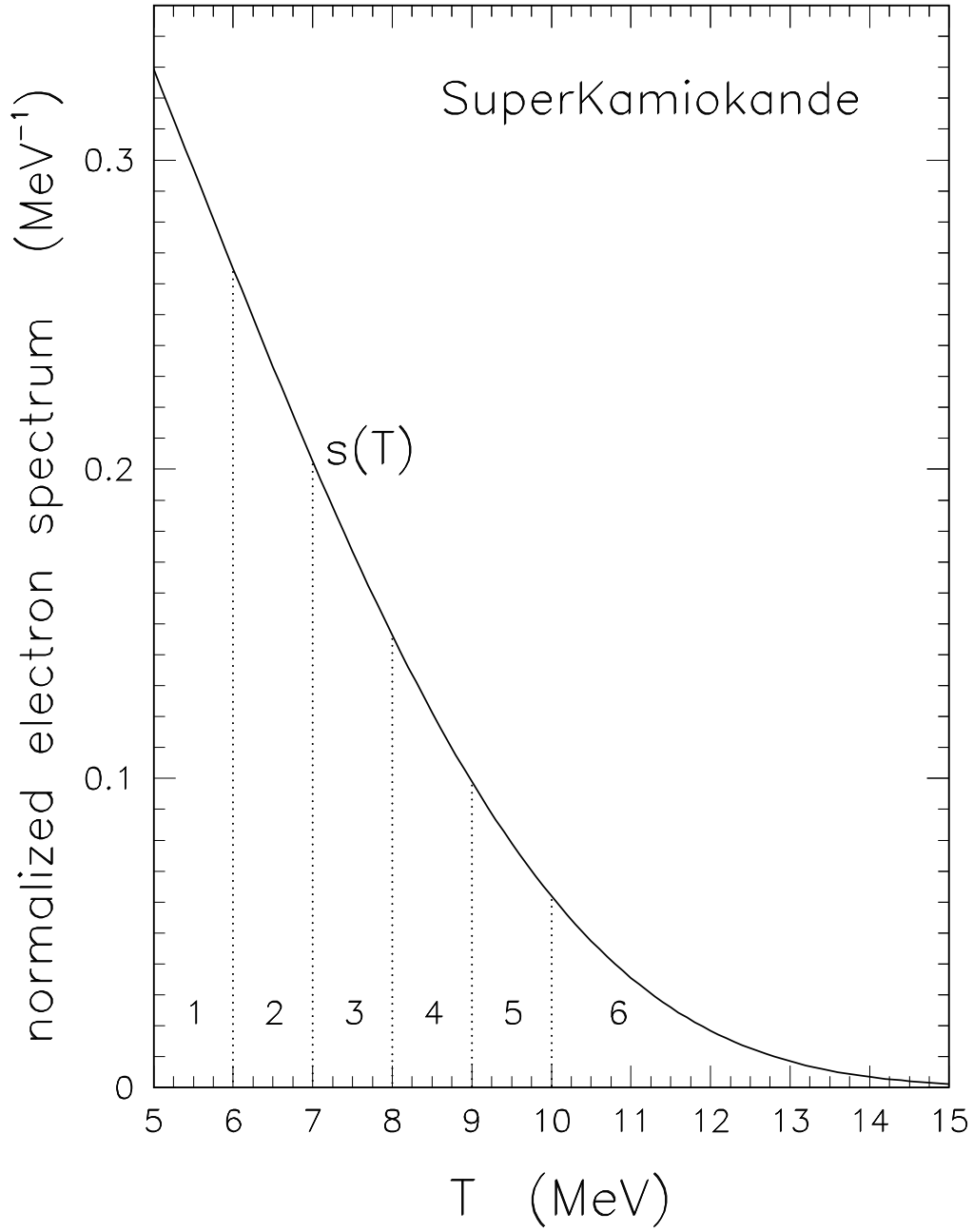


FIG. 2. SuperKamiokande: Standard electron spectrum  $s(T)$  as a function of the measured electron kinetic energy  $T$ . The area under  $s(T)$  is normalized to 1. Also shown are the (numbered) energy bins used in the analysis of  $A_{NF}$ .

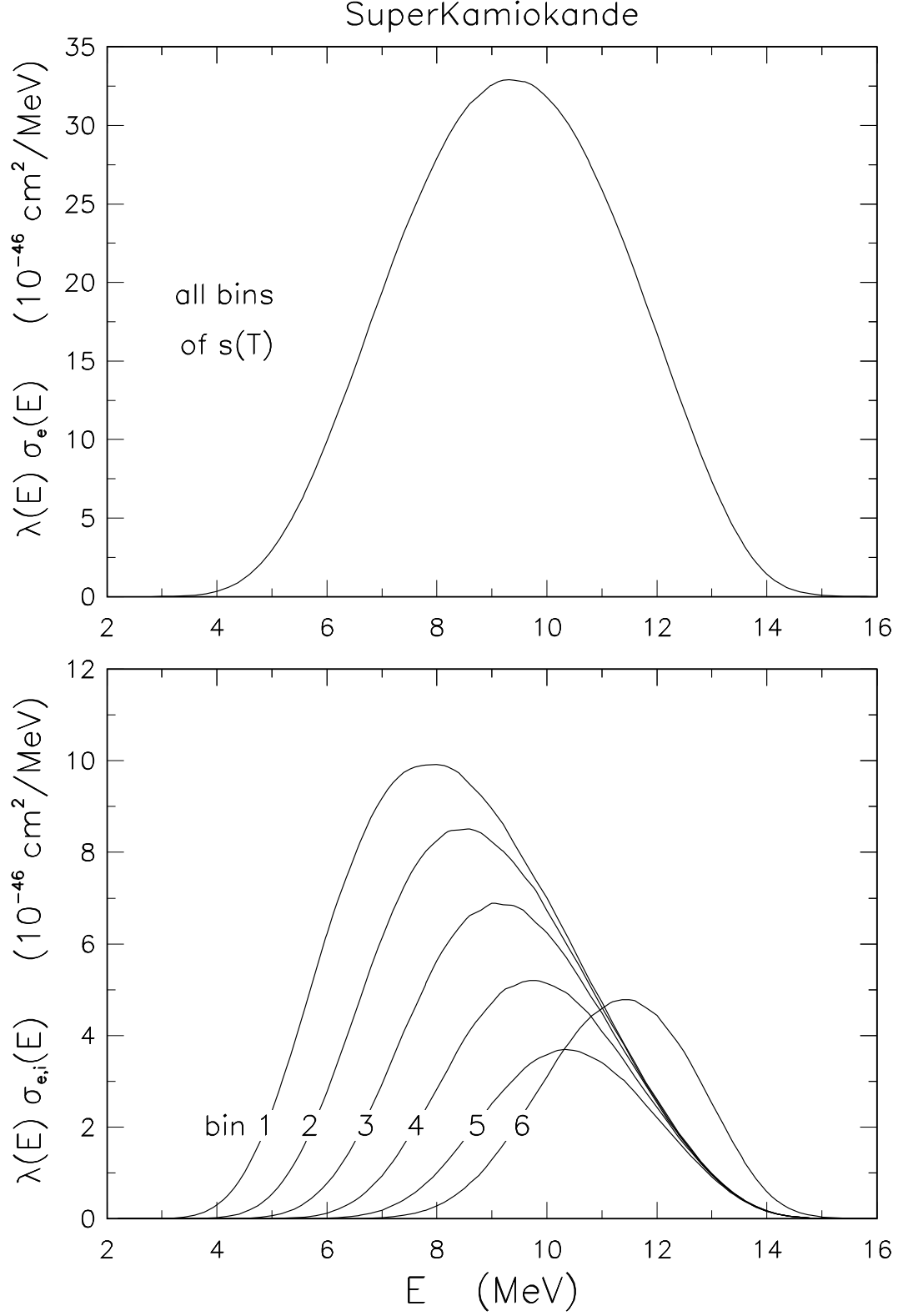


FIG. 3. SuperKamiokande: Spectra of  $\nu_e$  contributing to the entire standard electron spectrum of Fig. 2 or to selected bins. The neutrino spectra are weighted by the interaction cross sections, taking into account the detector threshold and the energy resolution function.

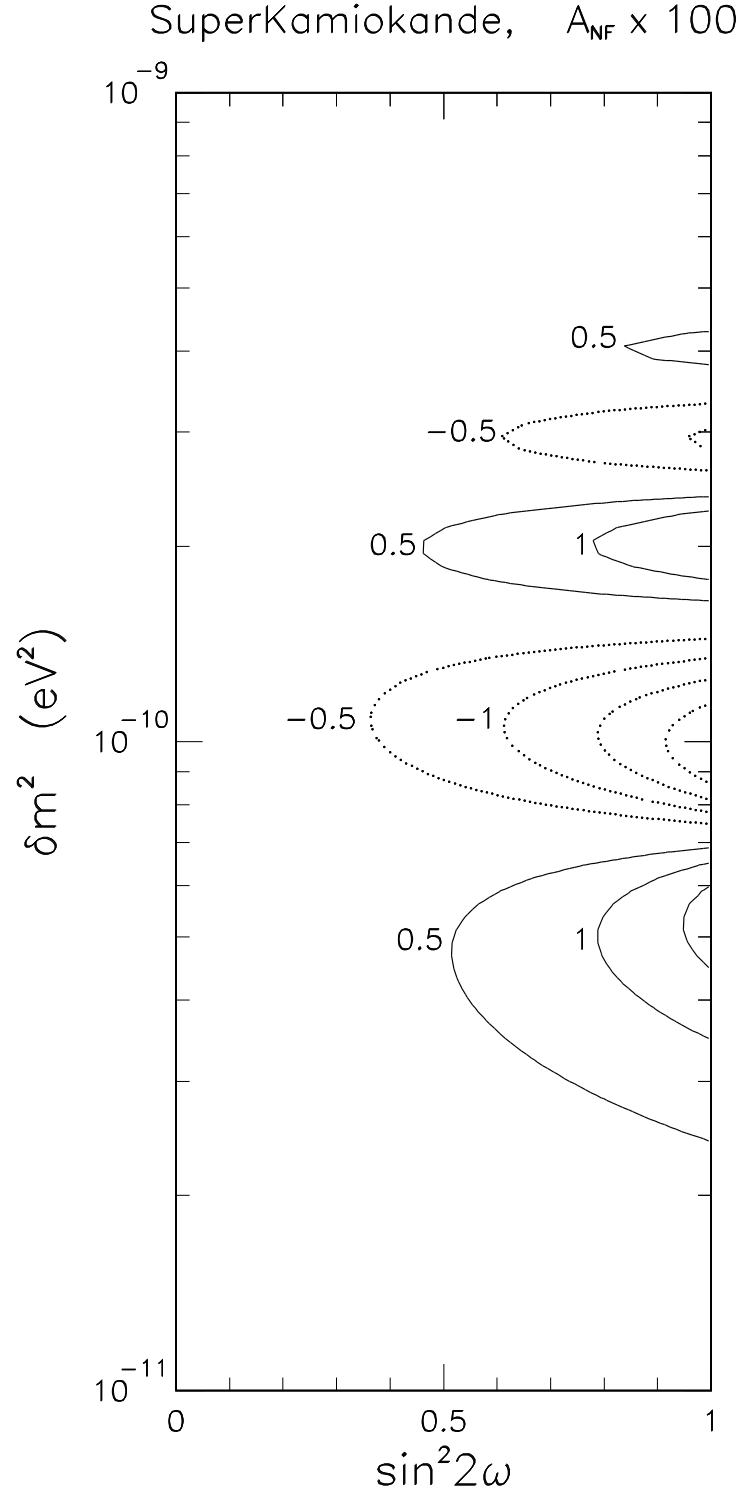


FIG. 4. SuperKamiokande: Curves of iso- $A_{NF}$  for  $2\nu$  oscillations (all bins).

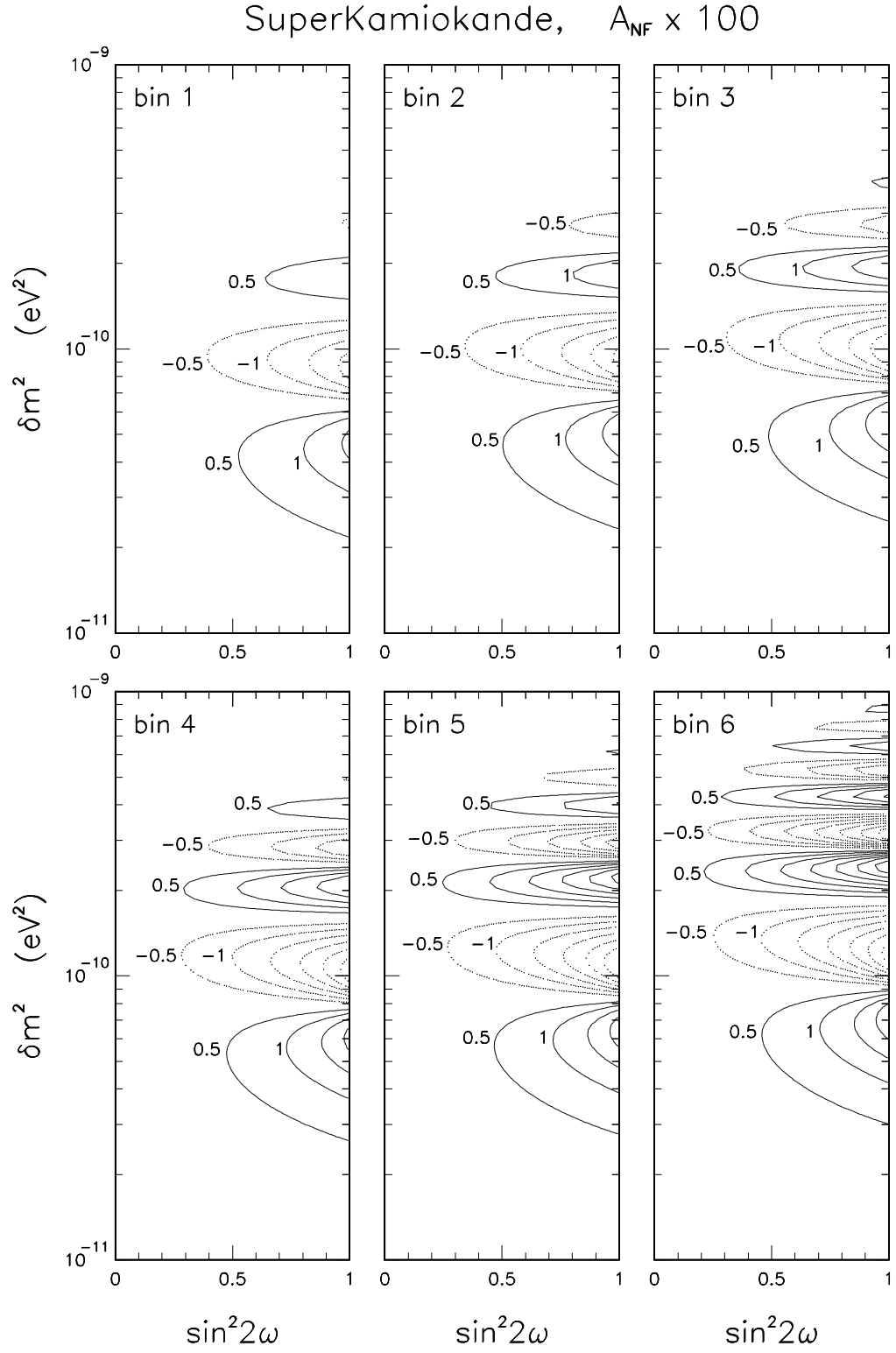


FIG. 5. SuperKamiokande: Curves of iso- $A_{NF}$  for  $2\nu$  oscillations (separated bins).

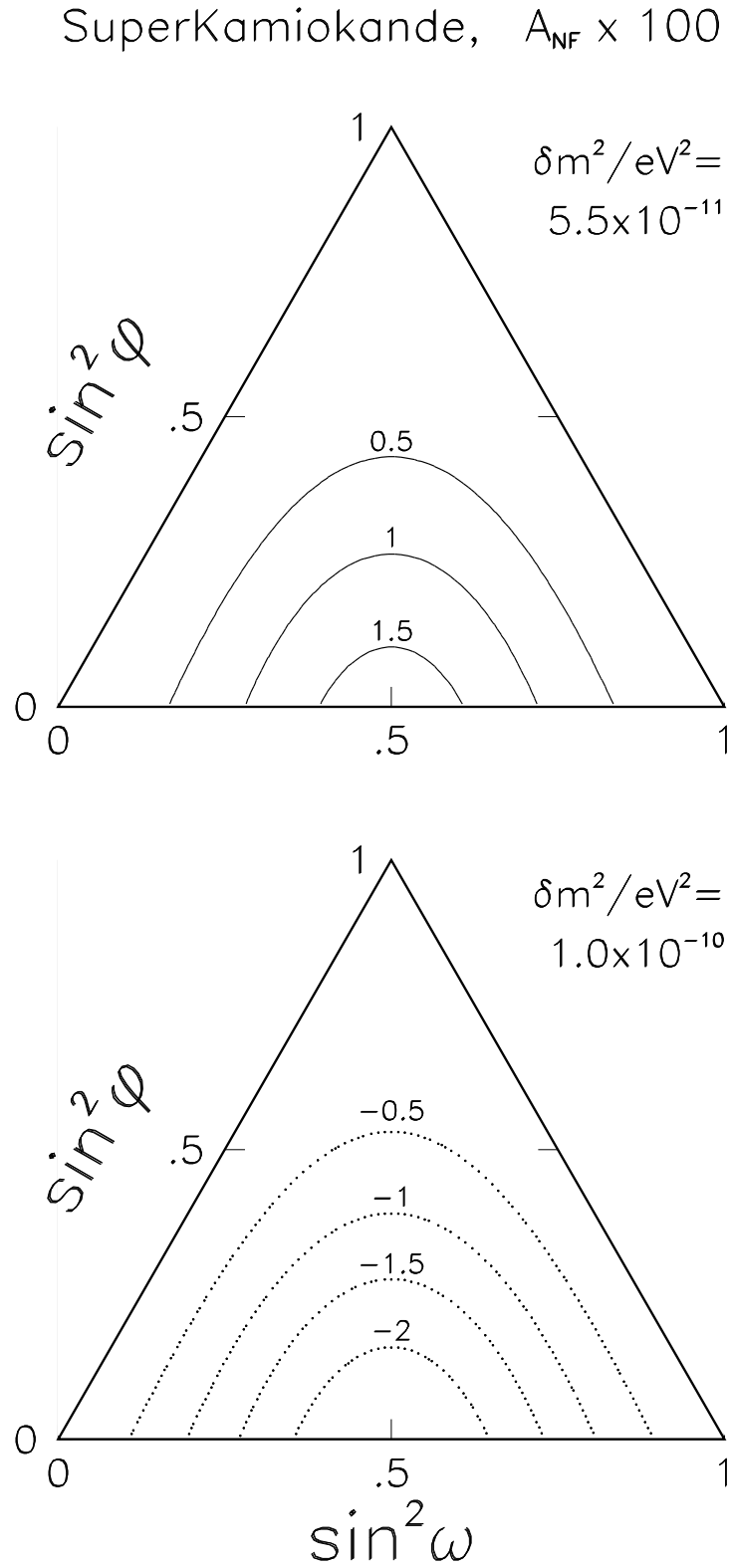


FIG. 6. SuperKamiokande: Curves of iso- $A_{\text{NF}}$  for  $3\nu$  oscillations (all bins), for two representative values of  $\delta m^2$ . The triangular representation is discussed in the text.

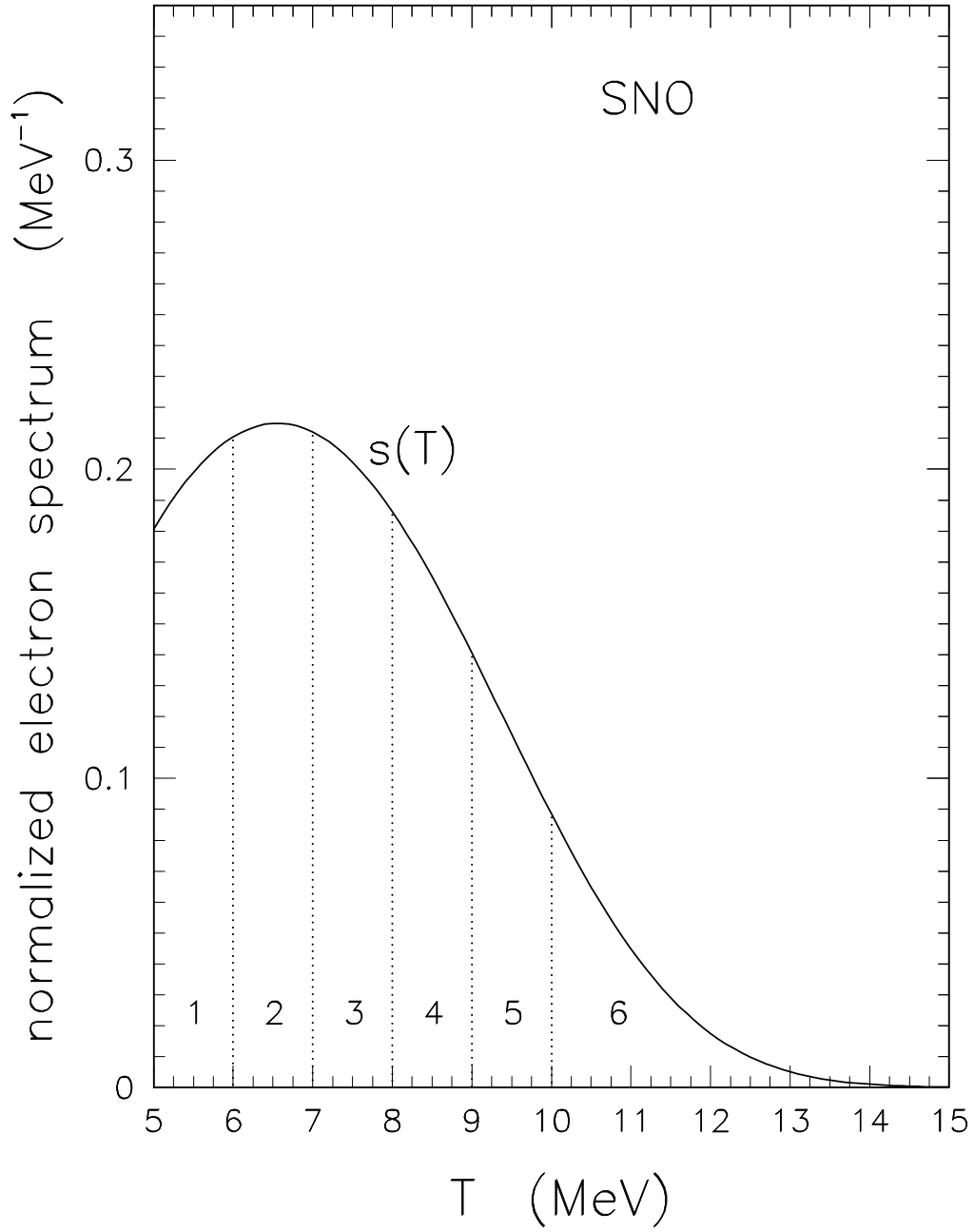


FIG. 7. SNO: Standard electron spectrum  $s(T)$  as a function of the measured electron kinetic energy  $T$ . The area under  $s(T)$  is normalized to 1. Also shown are the (numbered) energy bins used in the analysis of  $A_{NF}$ .



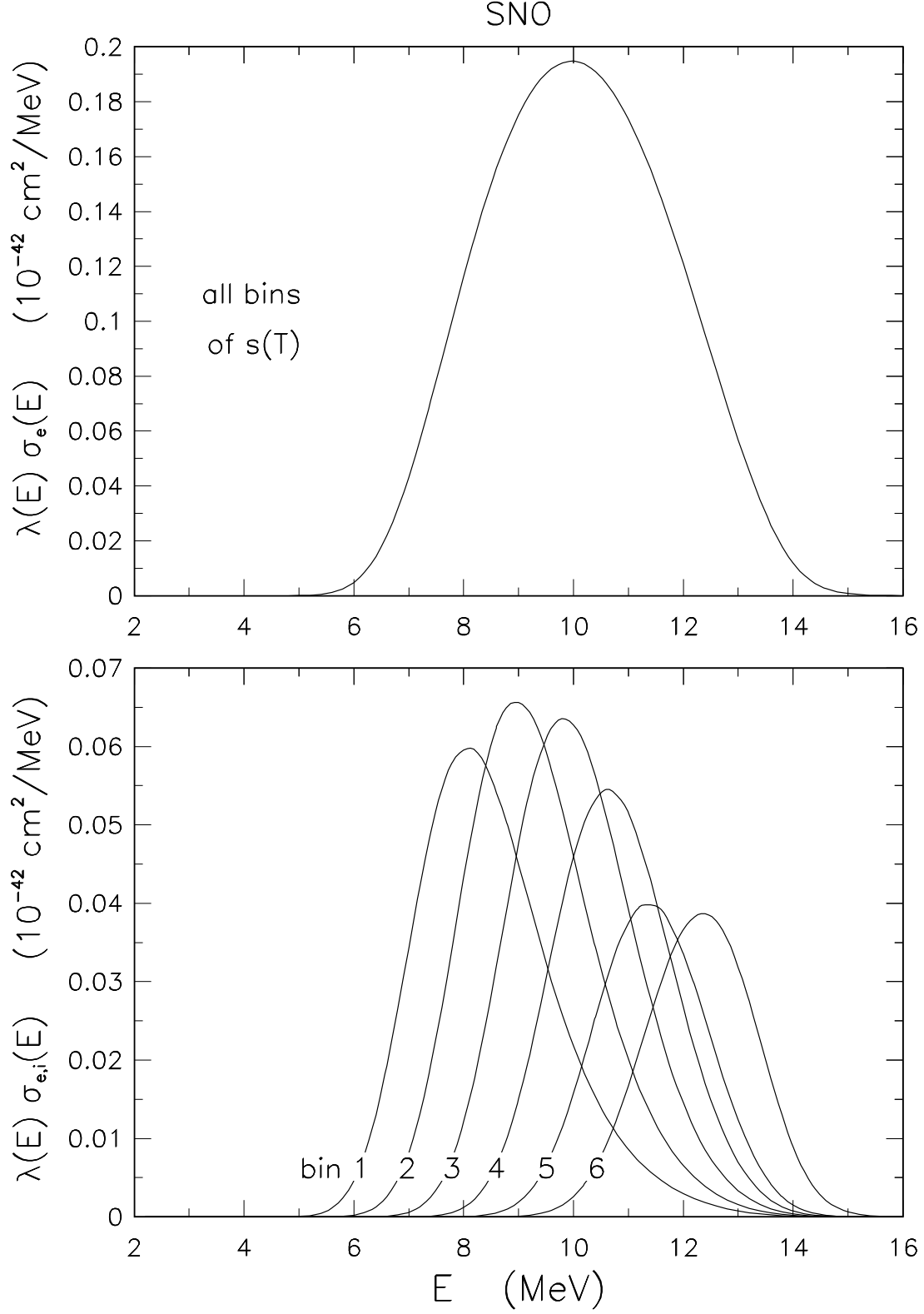


FIG. 8. SNO: Spectra of  $\nu_e$  contributing to the entire standard electron spectrum of Fig. 7 or to selected bins. The neutrino spectra are weighted by the interaction cross sections, taking into account the detector threshold and the energy resolution function.

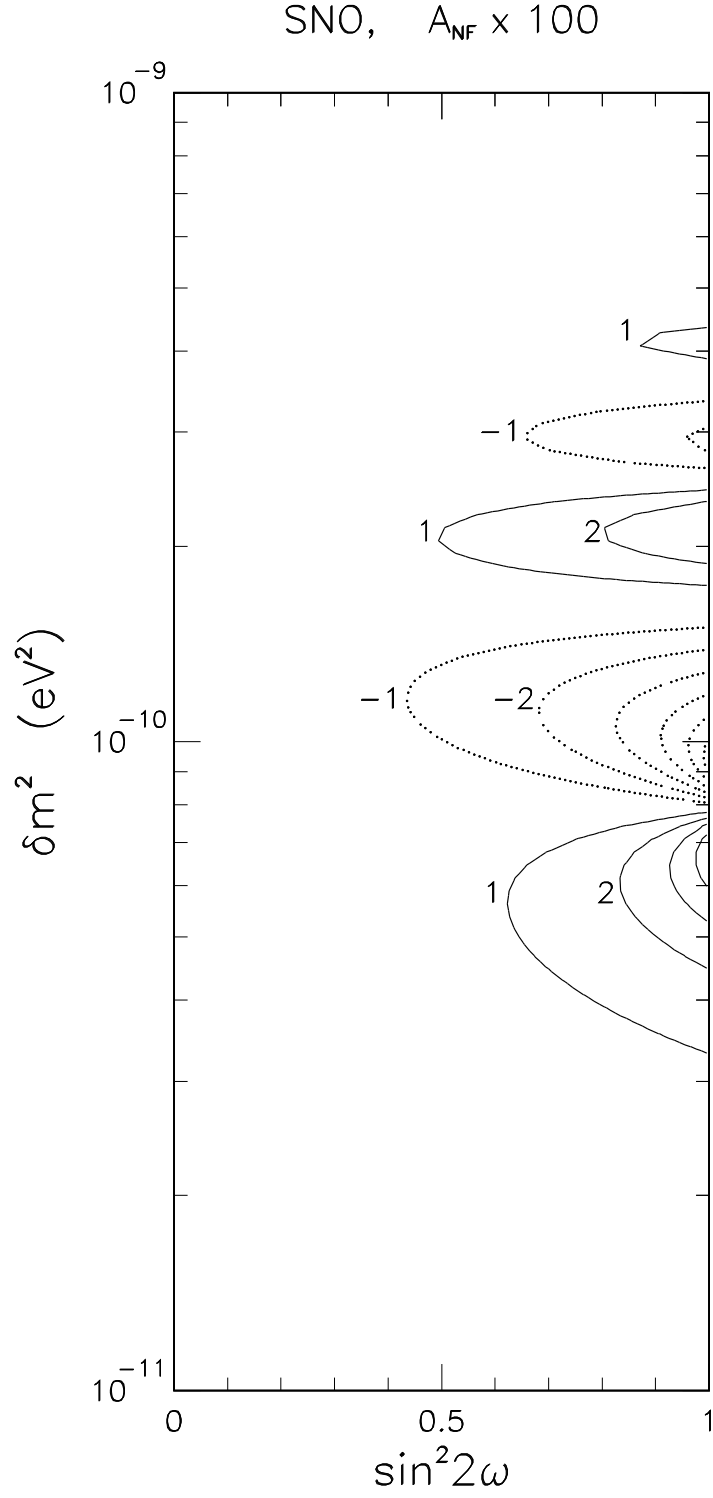


FIG. 9. SNO: Curves of iso- $A_{\text{NF}}$  for  $2\nu$  oscillations (all bins).

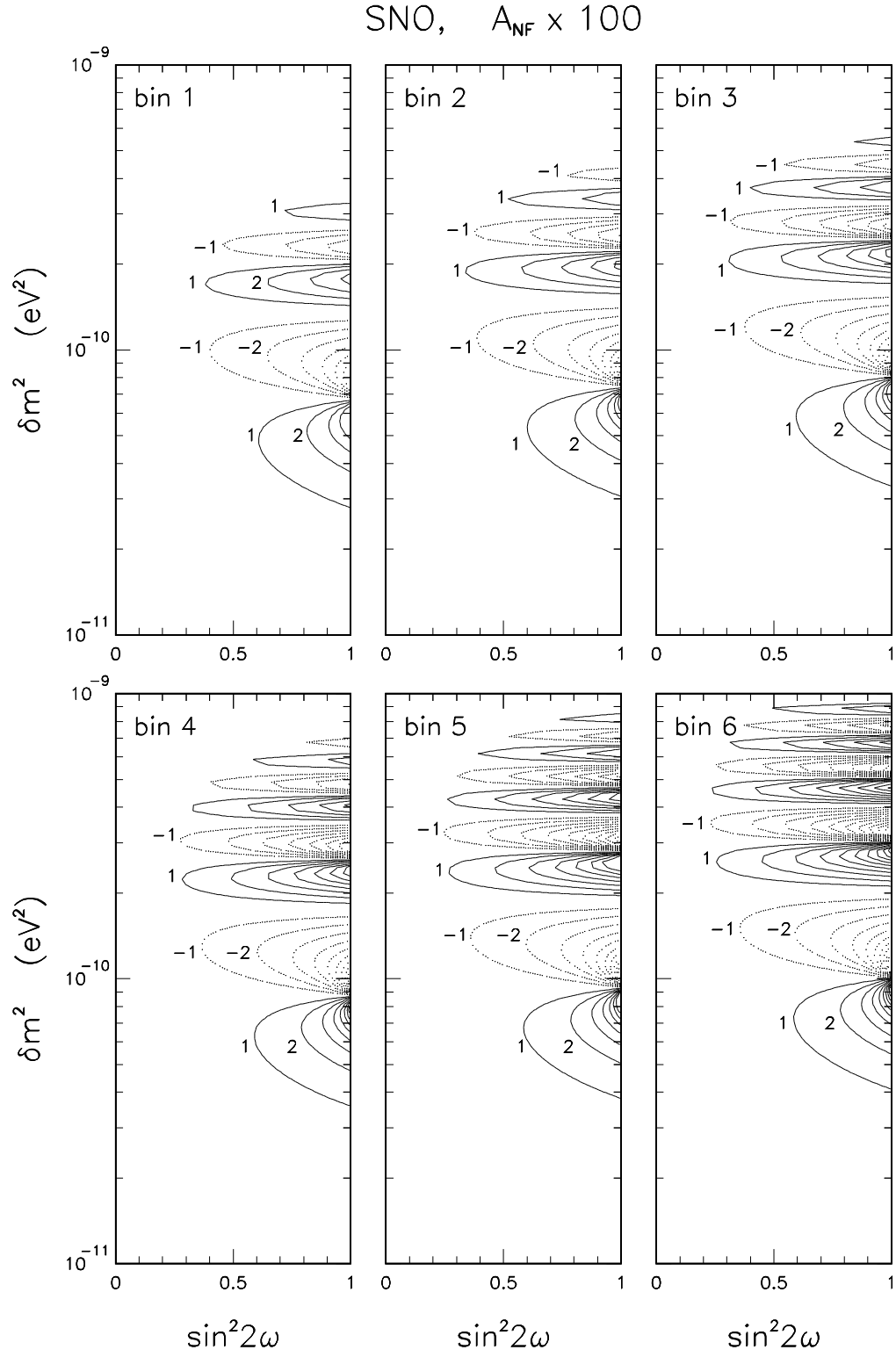


FIG. 10. SNO: Curves of iso- $A_{\text{NF}}$  for  $2\nu$  oscillations (separated bins).

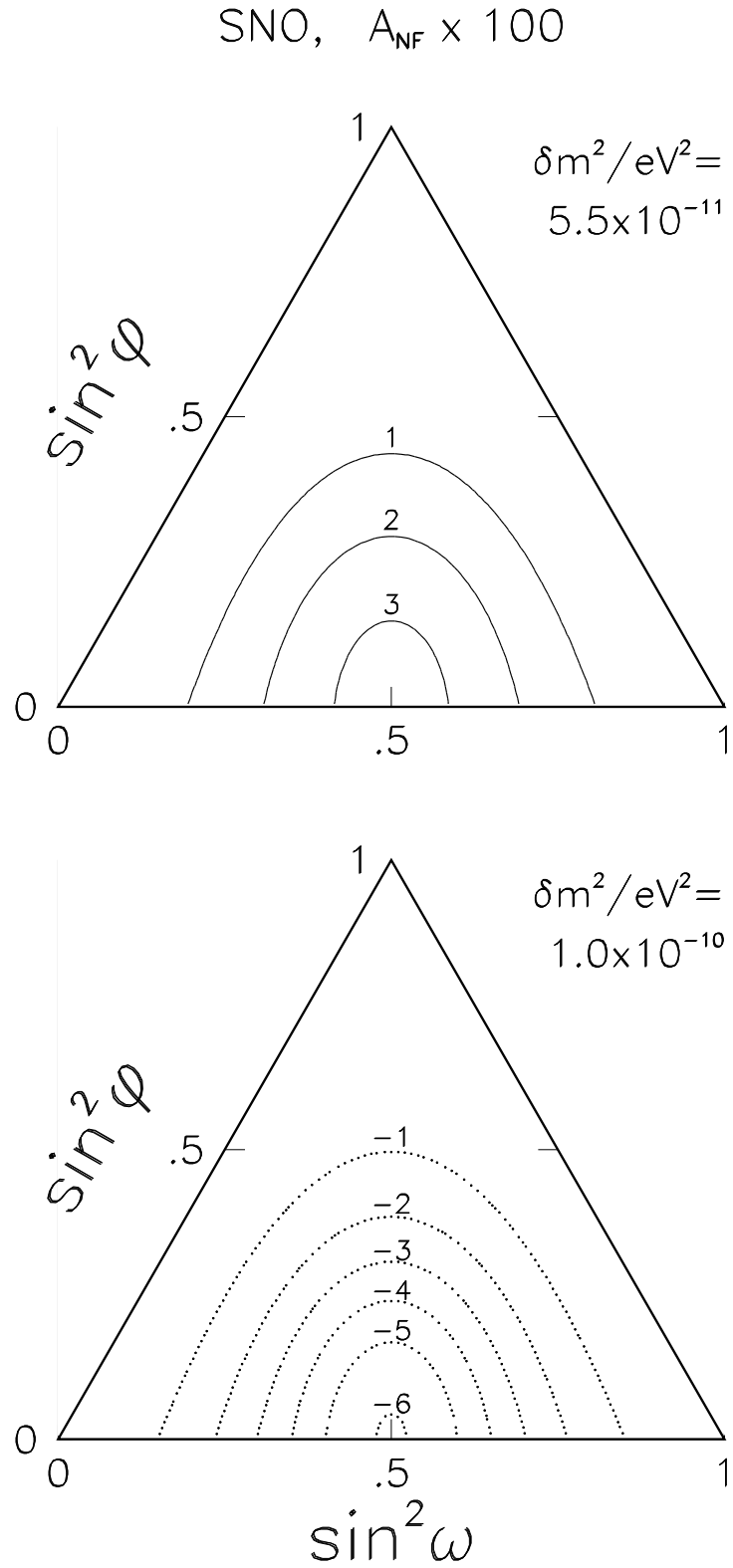


FIG. 11. SNO: Curves of iso- $A_{NF}$  for  $3\nu$  oscillations (all bins), for two representative values of  $\delta m^2$ . The triangular representation is discussed in the text.